



UNIVERSITÀ POLITECNICA DELLE MARCHE  
Repository ISTITUZIONALE

Insights into the fate of antimony (Sb) in contaminated soils: ageing influence on Sb mobility, bioavailability, bioaccessibility and speciation

This is the peer reviewed version of the following article:

*Original*

Insights into the fate of antimony (Sb) in contaminated soils: ageing influence on Sb mobility, bioavailability, bioaccessibility and speciation / Castaldi, Paola; Garau, Giovanni; Albert, Juhasz; Diquattro, Stefania; Ritch, Susie; Enzo, Lombi; Brunetti, Gianluca; Scheckel Kirk, G. - In: SCIENCE OF THE TOTAL ENVIRONMENT. - ISSN 0048-9697. - 770:(2021). [10.1016/j.scitotenv.2021.145354]

*Availability:*

This version is available at: 11566/315449 since: 2024-05-13T15:24:39Z

*Publisher:*

*Published*

DOI:10.1016/j.scitotenv.2021.145354

*Terms of use:*

The terms and conditions for the reuse of this version of the manuscript are specified in the publishing policy. The use of copyrighted works requires the consent of the rights' holder (author or publisher). Works made available under a Creative Commons license or a Publisher's custom-made license can be used according to the terms and conditions contained therein. See editor's website for further information and terms and conditions.

This item was downloaded from IRIS Università Politecnica delle Marche (<https://iris.univpm.it>). When citing, please refer to the published version.

(Article begins on next page)

1    **Insights into the fate of antimony (Sb) in contaminated soils: ageing influence on**  
2    **Sb mobility, bioavailability, bioaccessibility and speciation**

3

4    Stefania Diquattro<sup>a</sup>, Paola Castaldi<sup>a</sup>, Susie Ritch<sup>b</sup>, Albert L. Juhasz<sup>b</sup>, Gianluca  
5    Brunetti<sup>b</sup>, Kirk G. Scheckel<sup>c</sup>, Giovanni Garau<sup>a\*</sup>, Enzo Lombi<sup>b</sup>

6

7    <sup>a</sup> Dipartimento di Agraria, University of Sassari, Viale Italia 39/B, 07100, Sassari,  
8    Italy

9

10    <sup>b</sup> Future Industries Institute, University of South Australia, Mawson Lakes Campus,  
11    Adelaide, SA, 5095, Australia

12

13    <sup>c</sup> U. S. Environmental Protection Agency, Office of Research and Development,  
14    Center for Environmental Solutions and Emergency Response, Cincinnati, OH  
15    45268, United States

16

17    \* Corresponding author: G. Garau ([ggarau@uniss.it](mailto:ggarau@uniss.it))

18

19

20    **Abstract**

21

22    The effect of long-term ageing (up to 700 days) on the mobility, potential  
23    bioavailability and bioaccessibility of antimony (Sb) was investigated in two soils  
24    (S1: pH 8.2; S2: pH 4.9) spiked with two Sb concentrations (100 and 1000 mg·kg<sup>-1</sup>).

25 The Sb mobility decreased with ageing as highlighted by sequential extraction, while  
26 its residual fraction significantly increased. The concentration of Sb ( $C_{DGT}$ ), as  
27 determined by diffusive gradients in thin films (DGT), showed a reduction in  
28 potential contaminant bioavailability during ageing. The DGT analysis also showed  
29 that Sb- $C_{DGT}$  after 700 days ageing was significantly higher in S1-1000 compared to  
30 S2-1000, suggesting soil pH plays a key role in Sb potential bioavailability. In-vitro  
31 tests also revealed that Sb bioaccessibility decreased over time. Linear combination  
32 fitting of Sb K-edge XANES derivative spectra showed, as a general trend, an  
33 increase in Sb(V) sorption to inorganic oxides with ageing as well as Sb(V) bound to  
34 organic matter (e.g. up to 27 and 37 % respectively for S2-100). The results indicated  
35 that ageing can alleviate Sb ecotoxicity in soil and that the effectiveness of such  
36 processes can be increased at acidic pH. However, substantial risks due to Sb  
37 mobility, potential bioavailability and bioaccessibility remained in contaminated  
38 soils even after 700 days ageing.

39  
40 *Keywords:* Ageing; Antimony; Potential bioavailability; Bioaccessibility; X-ray  
41 absorption near-edge structure (XANES) spectroscopy

## 42 43 **1. Introduction**

44  
45 Antimony (Sb) is a potentially toxic element (PTE), considered as a priority  
46 pollutant by the United States Environmental Protection Agency and the European  
47 Union (CEC, 1998; USEPA, 2009). Antimony concentration in the environment is  
48 related to both natural phenomena such as weathering, biological activity, or volcanic

activity and anthropogenic inputs (He et al., 2019). In recent years, Sb concentrations in the environment have considerably increased as a result of mining and smelting operations, waste incinerators, coal and petroleum combustion, spent ammunition, polyethylene terephthalate industries, battery factories, and use of pharmaceuticals and pesticides (e.g. Okkenhaug et al., 2016). In this context, knowledge of Sb mobility, potential bioavailability and bioaccessibility in soil is of primary importance for the assessment of ecological risk and potential human health impacts (Diquattro et al., 2020; Fu et al., 2016; Hammel et al., 2000).

Antimony mobility, bioavailability and bioaccessibility in soil depend on its speciation as well as on the pH, redox conditions, amount and type of colloids present and microbial populations (Luo et al., 2014; Wilson et al., 2010). Antimony commonly occurs in the environment as trivalent Sb(III) or pentavalent Sb(V) inorganic species, with antimonite  $[Sb(OH)_3]$  and antimonate  $[Sb(OH)_6^-]$  the most common Sb(III) and Sb(V) compounds, respectively (Kang et al., 2000). Antimonate is the predominant form present under aerobic and mildly reducing conditions (Filella et al., 2002; Filella et al., 2009; Telford et al., 2008) and its mobility in soil, in the 5.0-8.5 pH range, is generally greater than that of antimonite due to the negative charge of the former species [ $pK_a HSb(OH)_6 = 2.55$ ;  $pK_a Sb(OH)_3 = 11.8$ ] (Herath et al., 2017; Johnston et al., 2020).

Binding to soil colloid surfaces (e.g., organic matter, Fe, Al, and Mn oxyhydroxides) by specific and nonspecific adsorption reactions, as well as structural incorporation into Fe(III)-oxyhydroxide minerals, can have substantial influence on Sb mobility and bioavailability, eventually leading to contaminant attenuation (Wilson et al., 2010). For instance, it was shown that different humic substance

functional groups (e.g., -SH and -COOH groups) can interact with Sb(III) (Tella and Pokrovski, 2009). In regards to Sb(V), specific adsorption by humic acids under acid conditions can occur via the establishment of pentagonal or hexagonal rings involving Sb–O–C linkages (Sh et al., 2012; Steely et al., 2007; Tella and Pokrovski, 2012). Moreover, cationic metals within humic acids [e.g, Fe(III), Mg(II), and Ca(II)], can act as bridging elements between the negatively charged humic molecules and the antimonate complex (Diquattro et al., 2018). Finally, stable interactions (e.g., inner sphere complexes) between Sb(V) and Fe and Al oxyhydroxides have previously been reported (Bagherifam et al., 2014; Essington and Stewart, 2016; 2018), as well as structural Sb(V) incorporation into Fe(III)-oxide (e.g. goethite) via heterovalent Sb(V)/Fe(III) substitution (e.g. Burton et al., 2020). Overall, the stability of complexes between Sb(V) and soil colloids decreases as the pH raises, due to the increase of electrostatic repulsion phenomena occurring between the  $\text{Sb(OH)}_6^-$  oxyanion and the negatively charged surface groups of Fe and Al oxy-hydroxides and organic matter (Xi et al., 2016). Moreover, the strength of Sb binding to soil colloid surfaces is fundamental in regulating contaminant bioaccessibility which is an important parameter for the prediction of exposure and health risks from incidental ingestion of Sb contaminated soils (Ruby et al., 1996). In particular, bioaccessibility refers to the fraction of a contaminant that is soluble in the digestive phase and as such potentially available for intestinal absorption (Mele et al., 2015).

Given that the stability of interactions between Sb and soil colloids, and therefore contaminant mobility, bioavailability and bioaccessibility, can change over time, this should be considered in order to gain a greater understanding of ecotoxicological

97 effects of antimony in soil systems and (more in general) in the environment  
98 (Violante et al., 2010). The reduction of PTEs mobility, potential bioavailability and  
99 bioaccessibility through specific immobilization mechanisms, which occur as a  
100 function of their contact time with soil colloids, is called “ageing” (e.g. Peng et al.,  
101 2019; Tang et al., 2006 ). Several PTEs-fixation reactions such as complexation,  
102 surface adsorption, precipitation or diffusion and occlusion into meso and  
103 micropores, can occur in soil with time (Jalali and Khanlari, 2008). For instance, lead  
104 (Pb), zinc (Zn), cadmium (Cd) and copper (Cu) tend to become non-exchangeable  
105 with an increase in residence time, due to the transformation of weak interactions  
106 (e.g. outer sphere complexes) into more stable ones (e.g. inner sphere complexes)  
107 (Jalali and Khanlari, 2008; Tang et al., 2006). Similarly, a decrease in water-soluble  
108 and exchangeable arsenic (As) and selenium (Se), and an increase in PTEs bound to  
109 amorphous Fe/Al oxy-hydroxides, or in residual fractions, have been observed  
110 during ageing (e.g. Peng et al., 2019; Tang et al., 2007).

111 Despite numerous studies over the last decade investigating the effects of ageing  
112 on the mobility and bioavailability of many PTEs (e.g. Diagboya et al., 2015;  
113 Martínez and McBride, 1998; Yang et al., 2003), limited knowledge is available for  
114 Sb. For instance, Sanderson et al. (2014) studied the bioavailability of Pb, Sb, Zn,  
115 nickel (Ni), Cu and As in soil after one year ageing, but the study mainly focused on  
116 selected ecotoxicological endpoints, i.e. earthworms, plants and microbial activity.  
117 Likewise, Zhang et al. (2020) explored Sb toxicity on barley root elongation after 3-  
118 months ageing, while Egodawatta et al. (2018) reported higher Sb bioavailability for  
119 water spinach when exposed to recently contaminated soil (14 days) compared to  
120 historically contaminated (34 years).

121 In this study we therefore sought to clarify the influence of ageing on the fate and  
122 behaviour of Sb in soil by using a combination of well-established and innovative  
123 approaches. More specifically, the objective of this work was to investigate the effect  
124 of ageing (from 1 day up to 700 days) on the mobility, potential bioavailability,  
125 bioaccessibility and speciation of Sb added [as Sb(V)] at two different concentrations  
126 (100 and 1000 mg·kg<sup>-1</sup>) on two distinct soils. In particular, the fate of Sb in soil was  
127 studied by sequential extraction to identify labile and relatively immobile Sb pools  
128 (Diquattro et al. 2020; Garau et al., 2017; Wenzel et al., 2001). Antimony potential  
129 bioavailability was addressed with diffusive gradients in thin-films (DGT) probes  
130 (Luo et al., 2010), while Sb bioaccessibility was studied by using simulated gastric  
131 and intestinal solutions in *in-vitro* tests (Ruby et al., 1996). Finally, synchrotron  
132 based X-ray absorption near-edge structure (XANES) spectroscopy was used to  
133 define Sb speciation in soil (Maher et al., 2018; Wang et al., 2017). The experimental  
134 design and the combined use of the above-mentioned techniques were expected to  
135 provide a deeper understanding of environmental risk posed by Sb and of possible  
136 attenuation mechanisms governed by time.

137

## 138 **2. Materials and methods**

139

### 140 *2.1. Soil physical-chemical analysis and microcosm set up*

141

142 Different topsoil samples (0-20 cm depth) were collected randomly from two  
143 uncultivated fields located in north-western Sardinia (Sassari), soil 1 (S1):  
144 40°43'32.77"N 8°24'48.6"E; soil 2 (S2): 40°56'15.7"N 8°53'30.4"E. These soils were

selected because they were not previously used for agricultural or anthropogenic activities, they were distant from possible contamination sources (i.e. to reduce the possibility of external Sb input), and they exhibited different physico-chemical properties (Table S1). Soil samples were pooled in the laboratory according to their origin (i.e., S1 and S2), sieved to < 2 mm and analysed as previously reported (Diquattro et al., 2020). Briefly, the S1 soil (sandy clay loam) was alkaline (pH 8.2), while S2 (loamy coarse sand) was acidic (pH 4.9). S1 had a higher cation exchange capacity (CEC) compared to S2, i.e. 20 vs 13  $\text{cmol}_{(+)}\cdot\text{kg}^{-1}$  soil respectively, while the opposite was found for soil organic matter (SOM), i.e. 1.75 vs 2.19 % and dissolved organic carbon (DOC), i.e. 0.17 vs 0.39  $\text{mg}\cdot\text{g}^{-1}$  soil respectively. The point of zero charge ( $\text{pH}_{\text{PZC}}$ ) was 5.7 for S1 and 2.6 for S2. High concentrations of total Fe (16,350 and 5,650  $\text{mg}\cdot\text{kg}^{-1}$  respectively) and Al (19,930 and 3,924  $\text{mg}\cdot\text{kg}^{-1}$  respectively) were recorded in S1 and S2, while total Ca was more abundant in S1 (62,500  $\text{mg}\cdot\text{kg}^{-1}$ ) compared to S2 (2,426  $\text{mg}\cdot\text{kg}^{-1}$ ). Antimony in S1 and S2 was quantified by Inductively Coupled Plasma Mass Spectrometry (ICP-QQQ-MS) (Agilent 8800) after digestion of soil with aqua regia reverse solution ( $\text{HNO}_3/\text{HCl}$  3:1 ratio) and microwave mineralisation (MARS-6, CEM) using USEPA method 3051A. A standard reference material (NIST-SRM 2711A) was included for quality assurance and quality control. In both soils, Sb was not detected (< 0.01  $\mu\text{g}\cdot\text{kg}^{-1}$ ). Further details on the chemical features of both soils can be found in Diquattro et al. (2020).

Thirty microcosms (each consisting of 300 g soil) were prepared for each soil type (S1 and S2) in plastic pots (10 cm diameter x 10 cm height). All soils were brought to 60 % of their water holding capacity (WHC) with deionised water (Jury et al., 1991). For each soil type, 15 microcosms were spiked with 100  $\text{mg}\cdot\text{kg}^{-1}$  Sb(V) (S-



100), and another 15 with 1000 mg·kg<sup>-1</sup> Sb(V) (S-1000). Sb(V) derived from K[Sb(OH)<sub>6</sub>] (CAS 12208-13-8; Sigma Aldrich, Saint-Louis, USA) was added as a water solution (K[Sb(OH)<sub>6</sub>] solubility in water is 20 g L<sup>-1</sup>). Antimony concentrations added were selected to mimic a medium-low and a high contamination level based on previous studies (Courtin-Nomade et al., 2012; Diquattro et al., 2020; Garau et al., 2017). Before addition to soil, each Sb(V) solution was adjusted to the same pH of the soil using 0.1 M NaOH or HCl solutions. Microcosms were carefully mixed and then left to age at constant temperature (25 °C) and humidity (60 % WHC; by weight adjustment) for different times: 1, 7, 31, 91 and 700 days (d). The selected time-points were chosen to evaluate both the short and medium to long-term influence of ageing on Sb mobility, bioavailability, bioaccessibility and speciation. At each time-point, triplicate S1 and S2 microcosms (i.e., S1-100, S1-1000, S2-100 and S2-1000) were analysed as follows. Total concentration of Sb was quantified in spiked microcosms (< 2 mm and < 250 µm particle size fractions) at different time-points (Table 1), by ICP-QQQ-MS as previously described. A standard reference material (NIST-SRM 2711A) was included for quality assurance and quality control.

185

## 186 2.2. Sequential extraction of soil Sb

187

188 At each time-point, Sb mobility in the different soils was evaluated through the  
189 sequential extraction procedure (SEP) proposed by Wenzel et al. (2001) with minor  
190 modifications. This method was originally developed for arsenic but has also been  
191 widely used for antimony (e.g. Diquattro et al., 2018; Garau et al., 2017; Ngo et al.,  
192 2020) because of the similar chemical characteristics of these PTEs (Wilson et al.,

2010). Different soil samples (n=10; 1 g each) were randomly collected from each microcosm and pooled together. Then a representative soil sample (1 g) was collected for Sb sequential extraction. The procedure was repeated 3 times for each microcosm. Triplicate soil samples (1 g) collected from each microcosm at different ageing times (i.e., 1, 7, 31, 91, 700 d) were treated with 25 mL of deionised water and shaken for 2 h at 25 °C to extract water-soluble Sb (Fraction 1, F1). Then, the same soil samples were treated with 25 mL of a 0.05 M (NH<sub>4</sub>)<sub>2</sub>SO<sub>4</sub> solution and shaken for 4 h at 25 °C to extract non-specifically sorbed Sb (Fraction 2, F2). Finally, the same soil samples were treated with 25 mL of a 0.05 M NH<sub>4</sub>H<sub>2</sub>PO<sub>4</sub> solution and shaken for 16 h at 25 °C to extract specifically sorbed Sb (Fraction 3, F3). Then, soil samples were digested with reverse aqua regia (HNO<sub>3</sub>/HCl 3:1 ratio) and microwave mineralisation (MARS-6, CEM) using USEPA method 3051A, to quantify residual Sb (Fraction 4, F4). After each extraction step, soil suspensions were centrifuged at 1800 g for 10 min. Supernatants were then filtered through a 0.45 µm filter and Sb concentrations determined in the liquid phase by ICP-QQQ-MS as previously described. A standard reference material (NIST-SRM 2711A) was included for quality assurance and quality control.

210

### 211 2.3. DGT measurements

212

213 At each time-point, Sb potential bioavailability was assessed in different soils  
214 through the DGT<sup>®</sup> technique. This is based on a device (deployed on the soil surface)  
215 that accumulates labile soil Sb on a binding gel after its diffusion through a hydrogel,  
216 which acts as a diffusion layer (Li et al., 2018). In this study, a titanium oxide

(Metsorb) binding gel (DGT Research Ltd, Lancaster, UK) was employed. The exposure area of the binding gel was 3.14 cm<sup>2</sup> and its thickness was 0.4 mm. Triplicate soil samples (50 g) collected from each microcosm at different ageing times (i.e., 1, 7, 31, 91,700 d) were brought to 100 % of their WHC, then a DGT device was deployed on the soil surface and gently pressed (to favour the contact between soil and device). DGT probes were left in contact with soils for 24 h at 25 °C. Afterwards, binding gels (of each DGT device) were collected and eluted for 24 h in 2 mL of a 1 M NaOH and 1 M H<sub>2</sub>O<sub>2</sub> solution. Eluent solutions were then 10-fold diluted in 2 % ultrapure HNO<sub>3</sub> prior to the analysis of Sb content by ICP-QQQ-MS as previously described.

The time-averaged Sb concentration present in the soil solution at the surface of the DGT device ( $C_{DGT}$ , expressed as  $\mu\text{g}\cdot\text{L}^{-1}$ ; i.e. a measure of labile or bioavailable soil Sb) was obtained according to the following equation (Eq. 1):

$$C_{DGT} = M\Delta g / AtD \quad (\text{Eq. 1}) \quad (\text{Davison and Zhang, 1994})$$

where M is the mass ( $\mu\text{g}$ ) of element accumulated on the binding gel,  $\Delta g$  is the thickness of the diffusive gel (0.8 mm) plus the thickness of filter membrane (0.1 mm), D is the element diffusion coefficient in the diffusive layer ( $5.46 \times 10^{-6} \text{ cm}^2 \text{ s}^{-1}$  for Sb; Luo et al., 2010), A is the exposed area of the binding gel (3.14 cm<sup>2</sup>), and t is the deployment time (s). Moreover, the R value, which reflects the ability of soil to resupply antimony to the device interface, was calculated as the ratio between Sb-DGT ( $C_{DGT}$ ) to Sb concentration in soil pore water ( $C_{sol}$ ) (Harper et al. 2000).

#### 2.4. *In vitro* bioaccessibility of soil Sb

At each time-point, Sb bioaccessibility in spiked soils was determined using the Solubility Bio-accessibility Research Consortium in vitro assay (SBRC) which includes a gastric (SBRC-G) and an intestinal phase (SBRC-I) (Mele et al., 2015). The  $< 250 \mu\text{m}$  (Table 1) soil particle size fraction was employed for analysis, since it represents the fraction that adheres to fingers and is available for incidental ingestion (Mele et al., 2015). Triplicate soil samples (0.4 g) collected (as described for SEP) from microcosms at different ageing times (i.e., 1, 7, 31, 91, 700 d) were treated with 40 mL of a gastric solution ( $30.03 \text{ g}\cdot\text{L}^{-1}$  glycine adjusted to pH 1.5 with 37 % HCl) and incubated in agitation (40 rpm on a Ratek rotary suspension mixer) at 37 °C and constant pH (i.e., 1.5). After 1-hour incubation, 4 mL of supernatant was collected, filtered through  $0.45 \mu\text{m}$  filters and stored at 4 °C (SBRC-G phase). The remaining suspension was adjusted to pH 7.0 with a 50 % NaOH solution, and intestinal solution (3 mL) containing 70 mg of bile bovine (Sigma-Aldrich) and 20 mg of pancreatin (Sigma-Aldrich) was added. The intestinal phase was then incubated at constant pH (i.e., 7.0) as previously mentioned. After 4 h, supernatant aliquots (10 mL) were collected, filtered through  $0.45 \mu\text{m}$  filters and stored at 4 °C (SBRC-I phase). Soluble Sb in SBRC-G and SBRC-I phases was determined by ICP-QQQ-MS (Agilent 8800), while total Sb concentration in soil was quantified after mineralization ( $< 250 \mu\text{m}$ ) as previously described. A standard reference material (SRM 2711A) was also included for quality assurance and quality control.

In vitro Sb bioaccessibility values (%) were calculated by dividing the Sb concentration determined in SBRC-G or SBRC-I phases by the total Sb concentration in the soil ( $< 250 \mu\text{m}$ ) as in the following equation (Eq. 2):

$$BA_{Sb} (\%) = [\text{soluble Sb in SBRC-G or SBRC-I (mg}\cdot\text{kg}^{-1}) / \text{total Sb concentration} \\ <250 \mu\text{m (mg}\cdot\text{kg}^{-1})] \times 100 \quad (\text{Eq. 2}).$$

266

## 267 2.5. X-ray absorption spectroscopy

268

269 Antimony K-edge X-ray absorption near-edge structure (XANES) spectra were  
 270 obtained to understand Sb speciation and its interaction with soil components during  
 271 ageing. XANES spectra were collected at the Materials Research Collaborative  
 272 Access Team's (MRCAT) beamline 10-BM (Kropf et al., 2010) at the Advanced  
 273 Photon Source (7 GeV storage ring in top-up mode), Argonne National Laboratory,  
 274 Argonne, IL (USA). Soil samples, collected at different ageing times (i.e., 1, 31, 700  
 275 d), were prepared by freeze drying, grinding with an agate mortar and pestle, and  
 276 pressing 75 mg of the sample in a 7-mm handheld pellet press. Samples from 7 and  
 277 91 d were not included in XANES analysis since SEP, DGT and SBRC data from  
 278 these time-points were similar to those at 31 and 700 d respectively. The sample  
 279 pellet was then encapsulated with Kapton tape and placed on a sample holder for  
 280 analysis. The beamline optics and setup parameters for the Sb edge XANES  
 281 measurements included calibration of the monochromator with a metallic Sb foil  
 282 (30491 eV) and the acquisition of metallic foil spectra with each sample scan for  
 283 spectral calibration verification. Data collection was conducted in both transmission  
 284 and fluorescence (4-element Vortex Si-drift detector) modes with gas purged ion  
 285 chambers for  $I_0$  (80% Ar/20% N<sub>2</sub>),  $I_{\text{Transmission}}$  (100% Ar), and  $I_{\text{Reference}}$  (100% Ar). At  
 286 least six scans for each sample were collected and it was evident fluorescence data  
 287 were of higher quality than transmission. Data analysis was conducted using Athena

software (Ravel and Newville, 2005). Multiple scans for each sample were aligned, merged, normalized, and calibration was performed by assigning the first inflection point of the reference Sb metal foil to 30491 eV. The relative abundance of Sb-bearing solid-phases was examined by linear combination fitting (LCF) of Sb K-edge XANES derivative spectra relative to known Sb reference samples (fitting range of -30 eV to +70 eV relative to the calibration energy). The  $\chi^2$  is a measure of the mean square sum of misfit at each data point and describes the degree of uncertainty in the fitting process (Ravel and Newville, 2005). Antimony reference standards included Sb<sub>2</sub>S<sub>3</sub>, Sb<sub>2</sub>O<sub>3</sub>, Sb(V)-tartrate, Sb(V)-citrate and KSb(OH)<sub>6</sub> (Sigma Aldrich, used for spike); Sb(V) and Sb(III) sorbed to goethite and Sb(III) sorbed to thiol-functionalised cellulose. Reference standards considered for LCF included Sb(V) sorbed to goethite to represent Sb(V) sorption by inorganic oxy-hydroxides (Essington and Stewart, 2018), Sb(V)-citrate to represent Sb(V) bound to organic matter, and KSb(OH)<sub>6</sub> to represent labile (e.g. water-soluble and exchangeable) Sb(V) in soil (Essington and Stewart, 2016). This latter interpretation was based on the high similarity of KSb(OH)<sub>6</sub> and Sb(OH)<sub>6</sub><sup>-</sup> spectra (e.g. Ji et al., 2017).

304

## 305 2.6. Statistical analysis

306

307 All chemical analyses were performed on triplicate soil samples collected from  
308 each mesocosm at different ageing times with mean values  $\pm$  standard errors reported  
309 in tables and figures. The Shapiro-Wilk test was performed in order to evaluate the  
310 normality of data distribution. For each soil (S1 or S2) and contamination level (100  
311 or 1000 mg·kg<sup>-1</sup>), the Fisher's LSD test was used to assess the influence of ageing

time on Sb mobility, potential bioavailability and bioaccessibility. Moreover, for each ageing time, comparisons between S1 and S2 at the same contamination level were made by using a Student t-test. Differences were considered statistically significant for  $P < 0.05$ . Pearson's correlation test was also performed to investigate the relationships between Sb concentrations recovered in the different steps of the SEP procedure, and those detected by DGT (i.e.  $C_{DGT}$ ) at different ageing times. Correlation values were considered statistically significant for  $P < 0.05$ . All statistical analyses were carried out using the Sigma Plot Software (SPSS Inc., Chicago, IL, USA).

### **3. Results and discussion**

#### *3.1. Influence of ageing on Sb mobility in contaminated soils*

To investigate the influence of ageing on the mobility of antimony in contaminated soils, different Sb fractions (or pools) characterised by a diverse degree of lability (i.e., solubility) were quantified at different time points. The water-soluble (i.e., highly mobile) Sb fraction (F1) decreased significantly over time for both soils and at both Sb concentrations (Fig. 1). The highest amounts of soluble Sb were detected at 1 d since spiking (40 and 18 % of total Sb for S1-100 and S2-100 and 24 and 26 % for S1-1000 and S2-1000 respectively), as previously reported elsewhere for other PTEs (e.g. Pb, Cu, Zn, Cd) (Jalali and Khanlari, 2008; Tang et al., 2006). Overall, such Sb amounts progressively and significantly reduced with ageing in both soils, even if different trends were observed depending on soil type and level of

contamination. In particular, significant reductions in water-soluble Sb occurred in all soils (with the exception of S2-100), after 7 d of ageing (Fig. 1). Interestingly, in S2-100, a significant reduction in soluble Sb occurred only at 91 d (Fig. 1). Such prolonged environmental stress could have favoured the development of an Sb-resistant bacterial community previously observed in this soil at 31 d ageing (Diquattro et al., 2020). The lowest amounts of soluble Sb were detected at 700 d of ageing even if, within each soil, the differences between 91 and 700 d were limited and, in some cases, not significant (Fig. 1). After 700 d ageing, soluble Sb was significantly reduced, compared to 1 d, by approx. 80 % in S1- and S2-100, and by 70 and 95 % in S1- and S2-1000 respectively. Taken together, these data indicate that 3 months ageing could be a suitable time for soil to equilibrate with aqueous Sb (i.e. very limited changes occurred after this time) and, consequently, to investigate the environmental fate of the contaminant and its ecotoxicological effects. Moreover, the higher Sb solubility observed in S1 compared with S2, especially after 700 d ageing (6 and 77 mg·kg<sup>-1</sup> in S1-100 and -1000 vs 4 and 13 mg·kg<sup>-1</sup> in S2-100 and -1000), could support previous research findings (Diquattro et al., 2020; Herath et al., 2017) where pH was identified as a key factor influencing Sb mobility. In particular, competition phenomena between hydroxide (OH<sup>-</sup>) and Sb(OH)<sub>6</sub><sup>-</sup> anions for Sb retention sites and/or repulsion between Sb(OH)<sub>6</sub><sup>-</sup> anions and negatively charged soil surfaces, could explain the higher Sb solubility in the alkaline S1 soil (pH 8.2) compared to the acidic S2 (pH 4.9). On the contrary, Fe/Al oxides and soil organic matter, i.e. other important sinks of soil Sb (Herath et al., 2017), seemed to play a limited or negligible role at influencing Sb mobility in these soils (Fe/Al content was much higher in S1, and SOM content was similar in S1 and S2).



360 After 1 d ageing, Sb extracted with  $(\text{NH}_4)_2\text{SO}_4$  (F2), i.e. the exchangeable pool,  
361 was significantly lower than water-soluble Sb in both soils (Fig. 1). Moreover, Sb  
362 extracted in F2 was significantly higher in S1-100 and -1000 (15.4 and 13.7 %)   
363 compared to S2-100 and -1000 (8.4 and 8.6 %), in agreement with the results of a  
364 recent short-term investigation based on the same soils (Fig. 1; Diquattro et al.,  
365 2020). Starting from 7 or 31 d, the amounts of exchangeable Sb significantly and  
366 progressively decreased (compared to 1 d) in all soils except S2-100 where a  
367 reduction was observed only at 700 d ageing (Fig. 1). Overall these data indicate a  
368 decrease of weaker (e.g. outer sphere) complexes and a concomitant increase of more  
369 specific (e.g. inner sphere) bonding between Sb and soil mineral and organic surfaces  
370 over time (Violante et al., 2010; Wenzel et al., 2001). As for the water-soluble F1  
371 fraction, this implied a Sb shift from more mobile (and potentially bioavailable)  
372 pools to less mobile (and hardly bioavailable) ones during ageing.

373 This was partly supported by Sb extracted with  $\text{NH}_4\text{H}_2\text{PO}_4$  (F3), i.e. Sb  
374 specifically sorbed by soil colloids (Wenzel et al., 2001). Such Sb pool can be  
375 considered as relatively mobile since it can be mobilised following a local pH change  
376 and/or a variation in P concentration (Wenzel et al., 2001). Antimony extracted in F3  
377 was generally low at day 1 (i.e., 10.2 and 7.6 % of total Sb for S1-100 and -1000, and  
378 3.7 and 2.3 % for S2-100 and -1000 respectively) which reduced (e.g. S1-100 and  
379 S2-1000) or remained constant (e.g. S1-100) during ageing (Fig. 1). The only  
380 exception was S1-1000 where Sb concentration slightly (yet significantly) increased  
381 with time, i.e. from 76 (at 1 d) to 81  $\text{mg}\cdot\text{kg}^{-1}$  soil (at 700 d) (Fig. 1).

382 Antimony detected in F4, i.e. residual Sb (e.g. associated with amorphous and  
383 crystalline Al and Fe oxy-hydroxides and/or precipitated or occluded), significantly

increased over time from 34, 70, 55 and 63 % at 1 d to 82, 79, 88 and 95 % at 700 d ageing in S1- and S2-100, and S1- and S2-1000 respectively (Fig. 1). This was in agreement with previous studies (e.g. Jalali and Khanlari, 2008; Peng et al., 2019) which reported an increase in residual PTEs such as Se, Pb, Cu, Cd, and Zn with ageing. However, the influence of ageing on Sb fractionation has been rarely addressed (e.g. Egodawatta et al., 2018; Zhang et al., 2020).

Taken together, SEP results highlighted a re-distribution of Sb from soluble (i.e., mobile) or weakly bound (easily mobilizable) forms, to less mobile and more stable ones during ageing. From an environmental viewpoint, this implies a time-dependent decrease in (micro)biological-impacting Sb fractions and an increase in less bioavailable forms.

### *3.2. Influence of ageing on Sb bioavailability in contaminated soils*

The diffusive gradient in thin film technique (DGT) was used to measure the flux of soluble Sb, which is supplied by diffusion through soil solution, as well as that of labile Sb resupplied by the soil solid phase to the DGT device (Letho, 2016). The diffusion of labile soil Sb (free and complexed soluble ions and weakly bound Sb species) into DGT devices has been previously shown to mimic the continuous uptake of PTEs by plant roots (Zhou et al., 2019). This is because, as pointed out by Zhang and Davison (2000), elemental flux to plant membranes and to DGT can be similar from a quantitative viewpoint (Letho et al., 2016). For this reason, the use of the DGT technique to estimate PTEs bioavailability to plants and soil (micro)biota has been steadily growing (e.g. Dai et al., 2018; Gu et al., 2017; Wang et al., 2019).

408 The  $C_{DGT}$  measurements showed that bioavailable Sb rapidly decreased at the  
409 initial stage of ageing (7-31 d) and reached an equilibrium at 91 d (in agreement with  
410 SEP results) in the majority of soils (Fig. 2). At low contamination levels (i.e., 100  
411  $\text{mg}\cdot\text{kg}^{-1}$ ), Sb bioavailability was always higher for soil S2 at all ageing times.  
412 However, after 700 d ageing, Sb- $C_{DGT}$  values in the pore water of the two soils were  
413 low and similar, i.e. 0.33 and 0.49  $\mu\text{g}\cdot\text{L}^{-1}$  (Fig. 2). This is relevant, as these  
414 concentrations are expected to pose limited threats for plants and soil (micro)biota  
415 (Geng et al., 2020; Sh et al., 2012). Nonetheless, it should be noted that much higher  
416 Sb- $C_{DGT}$  concentrations were detected during the previous time-points and this could  
417 have produced substantial perturbations of soil (micro)biological and biochemical  
418 features (e.g. Diquattro et al., 2020) whose effects could be still present after 700 d.  
419 In soils containing higher Sb concentrations (i.e., 1000  $\text{mg}\cdot\text{kg}^{-1}$ ), Sb bioavailability  
420 was significantly higher for soil S1 at all ageing times, with the exception of day 1  
421 (Fig. 2). After 700 d ageing, the Sb- $C_{DGT}$  in S1 was still 4.5-fold higher than in S2,  
422 and this supports higher Sb mobility detected by the SEP procedure in soil S1 (Fig.  
423 1). As previously mentioned, this could be attributed to the alkaline pH of soil S1  
424 and/or to the increased formation of stable Sb precipitates (e.g.  $\text{FeSbO}_4$  and  $\text{AlSbO}_4$ )  
425 in the acidic S2 (Dousova et al., 2018; Herath et al., 2017). It should be noted that, at  
426 low Sb contamination level (i.e., 100  $\text{mg}\cdot\text{kg}^{-1}$ ), this was not particularly evident as  
427 highlighted by both SEP and DGT results (Figs. 1-2). Overall, these results clearly  
428 indicate a steady reduction in Sb bioavailability during ageing, which also suggests a  
429 parallel increase in stable Sb-soil interactions over time, which was supported by  
430 SEP results.

431 The resupply of Sb from the solid phase to the soil pore water, i.e. R value ( $C_{DGT} /$   
432  $C_{sol}$ ), was low in both soils for all ageing times (i.e.,  $R < 0.12$  and  $< 0.05$  for S-100  
433 and S-1000 soils; Table 2) indicating that diffusion was the main process supplying  
434 Sb to the DGT device (Ma et al., 2020; Netho, 2016; Peng et al., 2019). Since the  
435 selected Sb fractions extracted by SEP are often correlated with the most labile (and  
436 potentially bioavailable) fractions in soil, i.e. those readily taken up by plants and  
437 soil microorganisms (e.g. Castaldi et al., 2018; Diquattro et al., 2018, 2020; Garau et  
438 al., 2017), the correlation between Sb- $C_{DGT}$  and that recovered in F1-F4 was tested  
439 (Table 3). Significant positive correlations were observed between F1 (0.786 –  
440 0.959;  $P < 0.01$ ), and F1+F2 (0.683 – 0.979;  $P < 0.01$ ), and Sb- $C_{DGT}$  while weaker  
441 relationships were recorded for F2 (Table 3). No significant relationship between Sb-  
442  $C_{DGT}$  and F3 was found, whereas significant negative correlations were observed  
443 between F4 (i.e., the less mobile and less bioavailable Sb) and Sb- $C_{DGT}$  (Table 3).

444 Taken together, these data highlight a good agreement between DGT and SEP  
445 results and confirmed the suitability of both approaches for the assessment of Sb  
446 mobility and potential bioavailability in soil. Overall, Sb- $C_{DGT}$  values showed that  
447 ageing had a marked influence on the potential bioavailability of Sb. This latter  
448 steadily decreased with time due to the conversion of Sb labile fractions into non-  
449 labile ones as indicated by SEP results.

450

### 451 3.3. Influence of ageing on Sb bioaccessibility

452

453 To investigate the influence of ageing on potential exposure for humans and  
454 animals related to incidental ingestion of Sb-contaminated soil, gastric and intestinal

phase Sb bioaccessibility was determined at different ageing times using the in vitro SBRC assay. Antimony bioaccessibility varied over time, and different trends were observed depending on soil type and Sb concentration (Fig. 3). When assessed using SBRC-G, Sb bioaccessibility significantly decreased with increasing ageing times with the exception of S1-100 when no variation in Sb bioaccessibility was recorded (Fig. 3). After 700 d ageing, Sb bioaccessibility in the SBRC-G phase was ~30, 26, 39 and 9 % (of total Sb present in the < 250 µm soil fractions) in S1- and S2-100, and S1- and S2-1000 respectively.

Considering that elemental absorption takes place in the intestinal compartment (Hamel et al., 1998), SBRC-I data are of particular interest. Antimony bioaccessibility in the SBRC-I phase quickly declined with ageing in the majority of soils (Fig. 3). In particular, significant reductions in bioaccessible Sb were recorded after 7 d for S2-1000 and after 31 d for S2-100 and S1-1000. However, it should be noted that after one day, Sb bioaccessibility in the SBRC-I phase was 46 % (of total Sb present in the < 250 µm soil fraction; Table 1) in S1-100 and between 61 and 72 % in the remaining soils (Fig. 3), that means an approx. 55 – 1800 mg Sb·kg<sup>-1</sup> soil. Nonetheless, ageing had a clear influence on Sb bioaccessibility (SBRC-I) which declined, compared to day 1, by a minimum of 15 % in S1-100, up to 60 % in S2-1000 (Fig. 3). Again, this supports a time-dependent increase of stable bonds between Sb and soil components (e.g. Fe oxy-hydroxides and organic matter), able to resist dissolution processes which take place during digestion (Denys et al., 2008). However, this was more pronounced for S2 soils where Sb binding to Fe/Al oxy-hydroxides and organic matter was likely favoured by the lower pH. Indeed, the acidic pH of the gastric phase commonly promotes the solubilisation of mineral

phases and the release of bonded PTEs, while the higher concentration of  $\text{OH}^-$  in the intestinal phase can prevent anion sorption/adsorption [e.g.  $\text{Sb}(\text{OH})_6^-$ ] by soil colloids which favours the release of further Sb into solution (Udovic and McBride, 2012).

Even if these results indicate a decreased Sb bioaccessibility over time, nonetheless, absolute Sb concentrations recorded in the SRBC-I phase at 700 d (i.e., 43 and 511  $\text{mg}\cdot\text{kg}^{-1}$  for S1-100 and S1-1000 respectively, and 90 and 367  $\text{mg}\cdot\text{kg}^{-1}$  for S2-100 and S2-1000) highlighted substantial potential health risks in both contaminated soils (Filella et al., 2002).

#### *3.4. Influence of ageing on Sb speciation*

Biogeochemical redox processes strongly influence Sb speciation, its interactions with soil colloids (and hence mobility and stability) as well as its toxicity. In this sense, spectroscopic techniques such as electron spin resonance (ESR) and X-ray absorption spectroscopy (XAS, including XANES) have been useful for the identification of metal and metalloid speciation and their complexes at surfaces of Al, Fe or Mn oxy-hydroxides, silicate clays and soil organic matter (Violante et al., 2010).

Derivative XANES spectra of Sb reference materials considered for LCF and of S1 and S2 soils are shown in Fig.s S1 and S2 respectively. LCF results for S1 and S2 samples (Table 4, Fig. S2) show the presence of labile Sb(V) (i.e.  $\text{KSb}(\text{OH})_6$  spectra) at varying degrees. Importantly, Sb(V) was the only redox state identified in XANES data. Labile Sb(V) concentration was higher for S1 samples than S2. Again, this

could be due to the influence of pH (8.2 vs 4.9, respectively) given the similar SOM content of S1 and S2 (1.75 and 2.19 %), and the higher Fe and Al content in the former soil (~ 3 and 5-fold respectively compared to S2). A similar influence of pH on Sb sorption by ferrihydrite was recently reported by Garau et al. (2019). Consistently, higher Sb-organic interactions (Sb(V)-citrate) and Sb sorbed to inorganic oxides (Sb(V)-goethite LCF reference) were recorded in S2 relative to S1 over time (Table 4). XANES spectroscopy is often not sensitive enough to distinguish if elements are sorbed by Fe or Al oxy-hydroxides in a complex soil matrix; however, spectra obtained are unique enough to distinguish them from organic complexes.

The initial concentration of Sb in each soil influenced final speciation results. S1-100 at 700 d resulted in Sb speciation components of 57 %  $\text{KSb(OH)}_6$  (which is indicative of labile  $\text{Sb(OH)}_6^-$ ), 18 % organic bound Sb(V), and 24 % sorbed to inorganic oxides; whereas S1-1000 at 700 d observed 81 %  $\text{KSb(OH)}_6$ , 14 % organic bound Sb(V), and 5 % sorbed to inorganic oxides. A similar trend was noted for the S2 concentration series where the  $\text{KSb(OH)}_6$  fraction was larger for the higher concentrated spiked sample.

#### **4. Conclusions**

Ageing had a clear influence on Sb mobility, bioavailability and bioaccessibility in contaminated soils. Labile (i.e., more soluble) Sb fractions progressively reduced during ageing indicating a decrease of weaker (e.g. outer-sphere) complexes and a concomitant increase of more specific (e.g. inner-sphere) bonding between Sb and

the soil components over time. This was accompanied by a parallel decrease of bioavailable and bioaccessible Sb which implied: i) a time-dependent increase of stable bonding between Sb and soil components and ii) a reduced ecotoxicological Sb impact on soil (micro)biota and humans with ageing. XANES LCF results indicated that Sb(V) was the only redox state present in soils during the almost 2-years experiment and that soil organic matter and Fe/Al oxy-hydroxides were the main sink of Sb during ageing. In this regard, soil pH appeared as a key parameter influencing the fate of Sb in our soils, i.e. Sb mobility, bioavailability and bioaccessibility were overall higher in the alkaline S1 soil compared to the acidic S2. Consistently, Sb fixation by soil organic matter and Fe/Al oxy-hydroxides was quantitatively less in S1 compared with S2 at all time-points considered. Nevertheless, absolute Sb concentrations recorded in the intestinal phase at 700 d highlight substantial potential health risks in both contaminated soils.

#### **Credit Author Statement**

**Stefania Diquattro:** Investigation, Methodology, Formal analysis, Writing - Original draft preparation. **Paola Castaldi:** Conceptualization, Formal analysis, Resources, Writing - Review & Editing. **Susie Ritch:** Methodology. **Albert L. Juhasz:** Resources, Formal analysis. **Gianluca Brunetti:** Methodology. **Kirk G. Scheckel:** Investigation, Formal analysis, Methodology, Writing - Review & Editing. **Giovanni Garau:** Conceptualization, Formal analysis, Writing - Review & Editing. **Enzo Lombi:** Conceptualization, Resources, Writing - Review & Editing, Project administration.



551

## 552 **Acknowledgements**

553

554 The financial support of the University of Sassari (Fondo di Ateneo per la Ricerca  
555 2019) is gratefully acknowledged.

556 MRCAT operations are supported by the Department of Energy and the MRCAT  
557 member institutions. This research used resources of the Advanced Photon Source, a  
558 U.S. Department of Energy (DOE) Office of Science User Facility operated for the  
559 DOE Office of Science by Argonne National Laboratory under Contract No. DE-  
560 AC02-06CH11357. Although EPA contributed to this article, the research presented  
561 was not performed by or funded by EPA and was not subject to EPA's quality system  
562 requirements. Consequently, the views, interpretations, and conclusions expressed in  
563 this article are solely those of the authors and do not necessarily reflect or represent  
564 EPA's views or policies.

565 The Future Industries Institute, University of South Australia is acknowledged for  
566 supporting this project.

567

## 568 **Appendix A. Supplementary data.**

569 Supplementary material related to this article is supplied as Table S1, Fig.s S1 and  
570 S2.

571

## 572    **References**

573

574    Bagherifam, S., Lakzian, A., Fotovat, A., Khorasani, R., Komarneni, S., 2014. In situ  
575        stabilization of As and Sb with naturally occurring Mn, Al and Fe oxides in a  
576        calcareous soil: Bioaccessibility, bioavailability and speciation studies. J.  
577        Hazard. Mater. 273, 247–252.

578    Castaldi, P., Diquattro, S., Lauro, G.P., Marceddu, S., Garau, G., 2018. Water  
579        treatment residuals as a resource for the recovery of soil and water polluted with  
580        Sb(V): sorption and desorption trials at different pH values. Water Air Soil  
581        Pollut. 229(6), 174.

582    CEC, 1998. Council Directive 98/83/EC of 3 November 1998 on the quality of water  
583        intended for human consumption (OJ L 330 05.12.1998 p. 32). In: Sands, P.,  
584        Galizzi, P. (Eds.), Documents in European Community Environmental Law.  
585        Cambridge University Press, Cambridge, pp. 865–878.

586    Courtin-Nomade, A., Rakotoarisoa, O., Bril, H., Grybos, M., Forestier, L., Foucher,  
587        F., Kunz, M., 2012. Weathering of Sb-rich mining and smelting residues:  
588        insight in solid speciation and soil bacteria toxicity. Chem. Erde-Geochem. 72,  
589        29–39.

590    Dai, Y., Nasir, M., Zhang, Y., Gao, J., Lv, Y., Lv, J., 2018. Comparison of DGT with  
591        traditional extraction methods for assessing arsenic bioavailability to *Brassica*  
592        *chinensis* in different soils. Chemosphere 191, 183–189.

593    Davison, W., Zhang, H., 1994. In situ speciation measurements of trace components  
594        in natural waters using thin-film gels. Nature 367, 546–548.

595    Denys, S., Tack, K., Caboche, J., Delalain, P., 2008. Bioaccessibility, solid phase  
596        distribution, and speciation of Sb in soils and in digestive fluids. Chemosphere  
597        74, 711–716.

598    Diagboya, P.N., Olu-Owolabi, B.I., Adebowale, K.O., 2015. Effects of aging, soil  
599        organic matter, and iron oxides on the relative retention of lead, cadmium, and  
600        copper on soils. Environ. Sci. Pollut. Res. 22, 10331–10339.

601    Diquattro, S., Garau, G., Lauro, G.P., Silvetti, M., Deiana, S., Castaldi, P., 2018.  
602        Municipal solid waste compost as a novel sorbent for antimony(V): adsorption  
603        and release trials at acidic pH. Environ. Sci. Pollut. Res. 25, 5603–5615.

604 Diquattro, S., Garau, G., Mangia, N.P., Drigo, B., Lombi, E., Vasileiadis, S.,  
605 Castaldi, P., 2020. Mobility and potential bioavailability of antimony in  
606 contaminated soils: Short-term impact on microbial community and soil  
607 biochemical functioning. *Ecotoxicol. Environ. Safe.* 196, 110576.

608 Dousova, B., Lhotka, M., Filip, J., Kolousek, D., 2018. Removal of arsenate and  
609 antimonate by acid-treated Fe-rich clays. *J. Hazard. Mater.* 357, 440–448.

610 Egodawatta, L.P., Macoustra, G.K., Ngo, L.K., Jolley, D.F., 2018. As and Sb are more  
611 labile and toxic to water spinach (*Ipomoea aquatica*) in recently contaminated soils  
612 than historically co-contaminated soils. *Environ. Sci. Proc. Imp.* 20, 833–844.

613 Essington, M.E., Stewart, M.A., 2016. Adsorption of antimonate by gibbsite:  
614 Reversibility and the competitive effects of phosphate and sulfate. *Soil Science*  
615 *Society of America Journal* 80, 1197–1207.

616 Essington, M.E., Stewart, M.A., 2018. Adsorption of antimonate, sulfate, and  
617 phosphate by goethite: Reversibility and competitive effects. *Soil Science*  
618 *Society of America Journal* 82, 803–814.

619 Filella, M., Belzile, N., Chen, Y.W., 2002. Antimony in the environment: A review  
620 focused on natural waters I. Occurrence. *Earth-Sci. Rev.* 57, 125–176.

621 Filella, M., Williams, P.A., Belzile, N., 2009. Antimony in the environment: Knowns  
622 and unknowns. *Environ. Chem.* 6, 95–105.

623 Garau, G., Silvetti, M., Vasileiadis, S., Donner, E., Diquattro, S., Deiana, S., Lombi,  
624 E., Castaldi, P., 2017. Use of municipal solid wastes for chemical and  
625 microbiological recovery of soils contaminated with metal(loid)s. *Soil Biol.*  
626 *Biochem.* 111, 25–35.

627 Garau, G., Lauro, G.P., Diquattro, S., Garau, M., Castaldi, P., 2019. Sb(V)  
628 adsorption and desorption onto ferrihydrite: influence of pH and competing  
629 organic and inorganic anions. *Environ. Sci. Pollut. Res.* 26, 27268–27280.

630 Geng, L., Yang, Z., Xu, Z., 2020. Effects of antimony contamination in soil on the  
631 nutrient composition of three green leafy vegetables. *Journal Soil. Sediment.* 20,  
632 2217–2224.

633 Gu, X., Liu, Z., Wang, X., Luo, J., Zhang, H., Davison, W., Ma, L.Q., Xue, Y., 2017.  
634 Coupling biological assays with diffusive gradients in thin-films technique to  
635 study the biological responses of *Eisenia fetida* to cadmium in soil. *J. Hazard.*

636 Mater. 339, 340–346.

637 Hamel, S.C., Buckley, B., Lioy, P.J., 1998. Bioaccessibility of metals in soils for  
638 different liquid to solid ratios in synthetic gastric fluid. *Environ. Sci. Technol.*  
639 32, 358–362.

640 Hammel, W., Debus, R., Steubing, L., 2000. Mobility of antimony in soil and its  
641 availability to plants. *Chemosphere* 41, 1791–1798.

642 Harper, M.P., Davison, W., Tych, W., 2000. DIFS - a modelling and simulation tool  
643 for DGT induced trace metal remobilisation in sediments and soils. *Environ.*  
644 *Model. Softw.* 15, 55–66.

645 He, M., Wang, N., Long, X., Zhang, C., Ma, C., Zhong, Q., Wang, A., Wang, Y.,  
646 Pervaiz, A., Shan, J., 2019. Antimony speciation in the environment: Recent  
647 advances in understanding the biogeochemical processes and ecological effects.  
648 *J. Environ. Sci. (China)* 75, 14–39.

649 Herath, I., Vithanage, M., Bundschuh, J., 2017. Antimony as a global dilemma:  
650 Geochemistry, mobility, fate and transport. *Environ. Pollut.* 223, 545–559.

651 Jalali, M., Khanlari, Z.V., 2008. Effect of aging process on the fractionation of heavy  
652 metals in some calcareous soils of Iran. *Geoderma* 143, 26–40.

653 Ji, Y., Sarret, G., Schulin, R., Tandy, S., 2017. Fate and chemical speciation of  
654 antimony (Sb) during uptake, translocation and storage by rye grass using  
655 XANES spectroscopy. *Environmental Pollution* 231, 1322–1329.

656 Johnston, S.G., Bennett, W.W., Doriean, N., Hockmann, K., Karimian, N., Burton,  
657 E.D., 2020. Antimony and arsenic speciation, redox-cycling and contrasting  
658 mobility in a mining-impacted river system. *Sci. Total Environ.* 710, 136354.

659 Jury, W., Gardner, W.R., Gardner, W.H. 1991. *Soil Physics*. 5<sup>th</sup> ed. John Wiley &  
660 Sons, New York.

661 Kang, M., Kawasaki, M., Tamada, S., Kamei, T., Magara, Y., 2000. Effect of pH on  
662 the removal of arsenic and antimony using reverse osmosis membranes.  
663 *Desalination* 131, 293–298.

664 Kropf, A.J., Katsoudas, J., Chattopadhyay, S., Shibata, T., Lang, E.A., Zyryanov,  
665 V.N., Ravel, B., McIvor, K., Kemner, K.M., Scheckel, K.G., Bare, S.R., Terry,  
666 J., Kelly, S.D., Bunker, B.A., Segre, C.U., 2010. The new MRCAT (Sector 10)  
667 Bending Magnet beamline at the Advanced Photon Source. *AIP Conference*

668        Proceedings 1234, 299–302.

669    Letho, N.J., 2016. Principles and application in soils and sediments. In: Davison, W.  
670        (Ed.), Diffusive gradients in thin-films for environmental measurements.  
671        Cambridge University Press, Padstow (United Kingdom), pp. 146–173.

672    Li, C., Ding, S., Yang, L., Wang, Y., Ren, M., Chen, M., Fan, X., Lichtfouse, E.,  
673        2018. Diffusive gradients in thin films: devices, materials and applications.  
674        Environ. Chem. Lett. 17, 801–831.

675    Li, J., Wei, Y., Zhao, L., Zhang, J., Shangguan, Y., Li, F., Hou, H., 2014.  
676        Bioaccessibility of antimony and arsenic in highly polluted soils of the mine  
677        area and health risk assessment associated with oral ingestion exposure.  
678        Ecotoxicol. Environ. Safe. 110, 308–315.

679    Luo, J., Bai, Y., Liang, J., Qu, J., 2014. Metagenomic approach reveals variation of  
680        microbes with arsenic and antimony metabolism genes from highly  
681        contaminated soil. PLoS One 9.

682    Luo, J., Zhang, H., Santner, J., Davison, W., 2010. Performance characteristics of  
683        diffusive gradients in thin films equipped with a binding gel layer containing  
684        precipitated ferrihydrite for measuring Arsenic(V), Selenium(VI),  
685        Vanadium(V), and Antimony(V). Anal. Chem. 82, 8903–8909.

686    Ma, X., Li, C., Yang, L., Ding, S., Zhang, M., Zhang, Y., Zhao, T., 2020. Evaluating  
687        the mobility and labile of As and Sb using diffusive gradients in thin-films  
688        (DGT) in the sediments of Nansi Lake, China. Sci. Total Environ. 713, 136569.

689    Maher, W.A., Krikowa, F., Foster, S.D., Ellwood, M.J., Bennett, W.W., 2018.  
690        Antimony measurements in environmental matrices: Seven considerations. J.  
691        Anal. At. Spectrom. 33, 706–712.

692    Martínez, C.E., McBride, M.B., 2001. Cd, Cu, Pb, and Zn coprecipitates in Fe oxide  
693        formed at different pH: Aging effects on metal solubility and extractability by  
694        citrate. Environ. Toxicol. Chem. 20, 122–126.

695    Mele, E., Donner, E., Juhasz, A.L., Brunetti, G., Smith, E., Betts, A.R., Castaldi, P.,  
696        Deiana, S., Scheckel, K.G., Lombi, E., 2015. In situ fixation of metal(loid)s in  
697        contaminated soils: a comparison of conventional, opportunistic, and engineered  
698        soil amendments. Environ. Sci. Technol. 49, 13501–13509.

699    Ngo, L.K., Price, H., Bennet, W.W., Teasdale, P.R., Jolley, D.F., 2020. DGT and

selective extractions reveal differences in arsenic and antimony uptake by the white icicle radish (*Raphanus sativus*). Environ. Pollut. 259, 113815.

Okkenhaug, G., Grasshorn Gebhardt, K.A., Amstaetter, K., Lassen Bue, H., Herzel, H., Mariussen, E., Rossebø Almås, Å., Cornelissen, G., Breedveld, G.D., Rasmussen, G., Mulder, J., 2016. Antimony (Sb) and lead (Pb) in contaminated shooting range soils: Sb and Pb mobility and immobilization by iron based sorbents, a field study. J. Hazard. Mater. 307, 336–343.

Peng, Q., Li, J., Wang, D., Wei, T.J., Chen, C.E.L., Liang, D.L., 2019. Effects of ageing on bioavailability of selenium in soils assessed by diffusive gradients in thin-films and sequential extraction. Plant Soil 436, 159–171.

Ravel, B., Newville, M., 2005. ATHENA, ARTEMIS, HEPHAESTUS: data analysis for X-ray absorption spectroscopy using IFEFFIT. J. Synchrotron Radiat. 12, 537–541.

Ruby, M.V., Davis, A., Schoof, R., Eberle, S., Sellstone, C.M., 1996. Estimation of lead and arsenic bioavailability using a physiologically based extraction test. Environ. Sci. Technol. 30, 422–430.

Sanderson, P., Naidu, R., Bolan, N., 2014. Ecotoxicity of chemically stabilised metal(loid)s in shooting range soils. Ecotoxicol. Environ. Safe. 100, 201–208.

Sh, T., Liu, C.Q., Wang, L., 2012. Antimony coordination to humic acid: Nuclear magnetic resonance and X-ray absorption fine structure spectroscopy study. Microchem. J. 103, 68–73.

Steely, S., Amarasiriwardena, D., Xing, B., 2007. An investigation of inorganic antimony species and antimony associated with soil humic acid molar mass fractions in contaminated soils. Environ. Pollut. 148, 590–598.

Tang, X.Y., Zhu, Y.G., Cui, Y.S., Duan, J., Tang, L., 2006. The effect of ageing on the bioaccessibility and fractionation of cadmium in some typical soils of China. Environ. Int. 32, 682–689.

Tang, X.Y., Zhu, Y-G, Shan, X-Q., McLaren, R., Duan, J., 2007. The ageing effect on the bioaccessibility and fractionation of arsenic in soils from China. Chemosphere 66, 1183–1190.

Telford, K., Maher, W., Krikowa, F., Foster, S., 2008. Measurement of total antimony and antimony species in mine contaminated soils by ICPMS and

732 HPLC-ICPMS. J. Environ. Monit. 10, 136–140.

733 Tella, M., Pokrovski, G.S., 2009. Antimony(III) complexing with O-bearing organic  
 734 ligands in aqueous solution: An X-ray absorption fine structure spectroscopy  
 735 and solubility study. Geochim. Cosmochim. Acta 73, 268–290.

736 Tella, M., Pokrovski, G.S., 2012. Stability and structure of pentavalent antimony  
 737 complexes with aqueous organic ligands. Chem. Geol. 292–293, 57–68.

738 Udovic, M., McBride, M.B., 2012. Influence of compost addition on lead and arsenic  
 739 bioavailability in reclaimed orchard soil assessed using *Porcellio scaber*  
 740 bioaccumulation test. J. Hazard. Mater. 205–206, 144–149.

741 USEPA, 2009. National Primary Drinking Water Regulations.

742 Violante, A., Cozzolino, V., Perelomov, L., Caporale, A.G., Pigna, M., 2010.  
 743 Mobility and bioavailability of heavy metals and metalloids in soil  
 744 environments. J. Soil Sci. Plant Nutr. 10, 268–292.

745 Yang J-K, Barnett M.O., Jardine P.M, Brooks S.C., 2003. Factors controlling the  
 746 bioaccessibility of arsenic(V) and lead(II) in soil. Soil Sediment Contam. 12(2),  
 747 165–179.

748 Wang, P., Lombi, E., Sun, S., Scheckel, K.G., Malysheva, A., McKenna, B.A.,  
 749 Menzies, N.W., Zhao, F.J., Kopittke, P.M., 2017. Characterizing the uptake,  
 750 accumulation and toxicity of silver sulfide nanoparticles in plants. Environ. Sci.  
 751 Nano 4, 448–460.

752 Wang, M., Cui, Z., Xue, M., Peng, Q., Zhou, F., Wang, D., Dinh, Q.T., Liu, Y.,  
 753 Liang, D., 2019. Assessing the uptake of selenium from naturally enriched soils  
 754 by maize (*Zea mays* L.) using diffusive gradients in thin-films technique (DGT)  
 755 and traditional extractions. Sci. Total Environ. 689, 1–9.

756 Wenzel, W.W., Kirchbaumer, N., Prohaska, T., Stingeder, G., Lombi, E., Adriano,  
 757 D.C., 2001. Arsenic fractionation in soils using an improved sequential  
 758 extraction procedure. Anal. Chim. Acta 436, 309–323.

759 Wilson, S.C., Lockwood, P. V., Ashley, P.M., Tighe, M., 2010. The chemistry and  
 760 behaviour of antimony in the soil environment with comparisons to arsenic: A  
 761 critical review. Environ. Pollut. 158, 1169–1181.

762 Xi, J., He, M., Kong, L., 2016. Adsorption of antimony on kaolinite as a function of  
 763 time, pH, HA and competitive anions. Environ. Earth Sci. 75, 1–7.

764 Zhang, H., Davison, W., 2000. Direct in situ measurements of labile inorganic and  
 765 organically bound metal species in synthetic solutions and natural waters using  
 766 diffusive gradients in thin films. *Anal. Chem.* 72, 4447.  
 767 Zhang, P., Wu, T.L., Ata-Ul-Karim, S.T., Ge, Y.Y., Cui, X., Zhou, D.M., Wang,  
 768 Y.J., 2020. Influence of soil properties and aging on antimony toxicity for  
 769 barley root elongation. *B. Environ. Contam. Tox.* 104, 714–720.  
 770 Zhou, J.W., Wu, L.H., Zhou, T., Li, Z., Sun, X.Y., Luo, Y.M., Christie P., 2019.  
 771 Comparing chemical extraction and a piecewise function with diffusive  
 772 gradients in thin films for accurate estimation of soil zinc bioavailability to  
 773 *Sedum plumbizincicola*. *Eur. J. Soil Sci.* 70, 1141–1152.  
 774



775 **Figure captions**

776

777 **Fig. 1.** Sequential extraction of antimony from S1 and S2 soils spiked with 100 (S-  
778 100) and 1000 (S-1000) mg Sb kg<sup>-1</sup> soil at different ageing time. For each Sb fraction  
779 (F<sub>x</sub>), different letters on top of each bar (e.g. a, b, c, d) denote ageing-dependent  
780 statistical differences (Fisher's LSD,  $P < 0.05$ ). For each Sb fraction and ageing time,  
781 asterisks denote statistical differences between S1-100 and S2-100, and between S1-  
782 1000 and S2-1000 soils (Student t-test,  $P < 0.05$ ).

783

784 **Fig. 2.** Antimony concentrations as obtained by DGT (Sb-C<sub>DGT</sub>) in S1 and S2 soils  
785 spiked with 100 (S-100) and 1000 (S-1000) mg Sb kg<sup>-1</sup> soil at different ageing time.  
786 For each soil, different letters on top of each bar (e.g. a, b, c, d) denote ageing-  
787 dependent statistical differences (Fisher's LSD,  $P < 0.05$ ). For each ageing time,  
788 asterisks denote statistical differences between S1-100 and S2-100, and between S1-  
789 1000 and S2-1000 soils (Student t-test,  $P < 0.05$ ).

790

791 **Fig. 3.** *In vitro* bioaccessibility of Sb in S1 and S2 soils spiked with 100 (S-100) and  
792 1000 (S-1000) mg Sb kg<sup>-1</sup> soil at different ageing time. For each soil, different letters  
793 on top of each bar (e.g. a, b, c, d) denote ageing-dependent statistical differences  
794 (Fisher's LSD,  $P < 0.05$ ). For each ageing time, asterisks denote statistical  
795 differences between S1-100 and S2-100, and between S1-1000 and S2-1000 soils  
796 (Student t-test,  $P < 0.05$ ). SBRC-G= bio-accessible Sb in the gastric phase; SBRC-I  
797 = bio-accessible Sb in the intestinal phase.

798

799 **Table S1.** Selected physico-chemical characteristics of S1 and S2 soils.

800

801 **Fig. S1.** Derivative XANES spectra of antimony reference materials considered for  
802 linear combination fitting.

803

804 **Fig. S2.** Derivative XANES spectra of antimony from S1 and S2 soils spiked with  
805 100 (S-100) and 1000 (S-1000) mg Sb kg<sup>-1</sup> soil at different ageing time. Black curves  
806 represent sample data while red curves represent LCF results. Processed results are  
807 presented in Table 4.

**Table 1**

Concentration of total Sb in < 250  $\mu\text{m}$  particle size fractions.

Time	Sb concentration ( $\text{mg kg}^{-1}$ )	
	<i>S1-100</i>	<i>S1-1000</i>
1 d	$121.1 \pm 2.51$	$1167 \pm 19.3$
7 d	$159.2 \pm 6.86$	$1384 \pm 9.64$
31 d	$119.0 \pm 5.99$	$1326 \pm 24.0$
91 d	$156.3 \pm 1.65$	$1321 \pm 22.3$
700 d	$139.0 \pm 4.25$	$1403 \pm 71.9$
	<i>S2-100</i>	<i>S2-1000</i>
1 d	$234.2 \pm 9.13$	$2500 \pm 47.2$
7 d	$237.9 \pm 7.94$	$2954 \pm 438$
31 d	$254.2 \pm 1.21$	$2734 \pm 250$
91 d	$297.0 \pm 30.2$	$2950 \pm 268$
700 d	$252.1 \pm 5.80$	$2956 \pm 287$

**Table 2**

Concentration of Sb in soil solution ( $C_{\text{sol}}$ ) and R values in soils during ageing.

Ageing time (d)	$C_{\text{sol}}$ ( $\mu\text{g}\cdot\text{L}^{-1}$ )				R value ( $R = C_{\text{DGT}}/C_{\text{sol}}$ )			
	S1-100	S2-100	S1-1000	S2-1000	S1-100	S2-100	S1-1000	S2-1000
1	88.88	38.06	535.6	596.6	0.049	0.119	0.045	0.050
7	28.83	37.44	300.3	91.2	0.039	0.068	0.035	0.049
31	27.64	39.11	260.3	72.2	0.036	0.046	0.033	0.039
91	13.33	16.73	212.3	35.3	0.039	0.061	0.030	0.038
700	15.76	8.84	173.0	26.6	0.021	0.056	0.028	0.041

**Table 3**

Pearson correlation coefficients (r) between the Sb fractions detected by SEP and those quantified by DGT ( $C_{DGT}$ ) in S1 and S2 soils <sup>†</sup>.

	S1-100	S1-1000	S2-100	S2-1000
	$C_{DGT}$	$C_{DGT}$	$C_{DGT}$	$C_{DGT}$
F1	0.959**	0.946**	0.786**	0.947**
F2	0.853**	0.911**	0.297 <sup>NS</sup>	0.780**
F1+F2	0.967**	0.979**	0.683**	0.966**
F3	0.425 <sup>NS</sup>	-0.106 <sup>NS</sup>	-0.041 <sup>NS</sup>	-0.032 <sup>NS</sup>
F4	-0.958**	-0.921**	-0.537*	-0.963**

<sup>†</sup> NS not significant ( $P > 0.05$ ); \* statistically significant at  $P < 0.05$ ; \*\* statistically significant at  $P < 0.01$ .

**Table 4**

Linear Combination Fitting (LCF)–XANES analysis of Sb speciation.

Sb speciation distribution (%)				
	KSb(OH) <sub>6</sub>	Sb(V)-Citrate	Sb(V)-Goethite	$\chi^2$
S1-100 1 d	88	12	0	0.0059
S1-100 31 d	63	19	18	0.0242
S1-100 700 d	57	18	24	0.0063
S2-100 1 d	55	32	13	0.0088
S2-100 31 d	43	36	21	0.0150
S2-100 700 d	36	37	27	0.0091
S1-1000 1 d	88	12	0	0.0022
S1-1000 31 d	85	12	3	0.0021
S1-1000 700 d	81	14	5	0.0034
S2-1000 1 d	62	25	13	0.0037
S2-1000 31 d	59	23	18	0.0014
S2-1000 700 d	58	21	21	0.0543

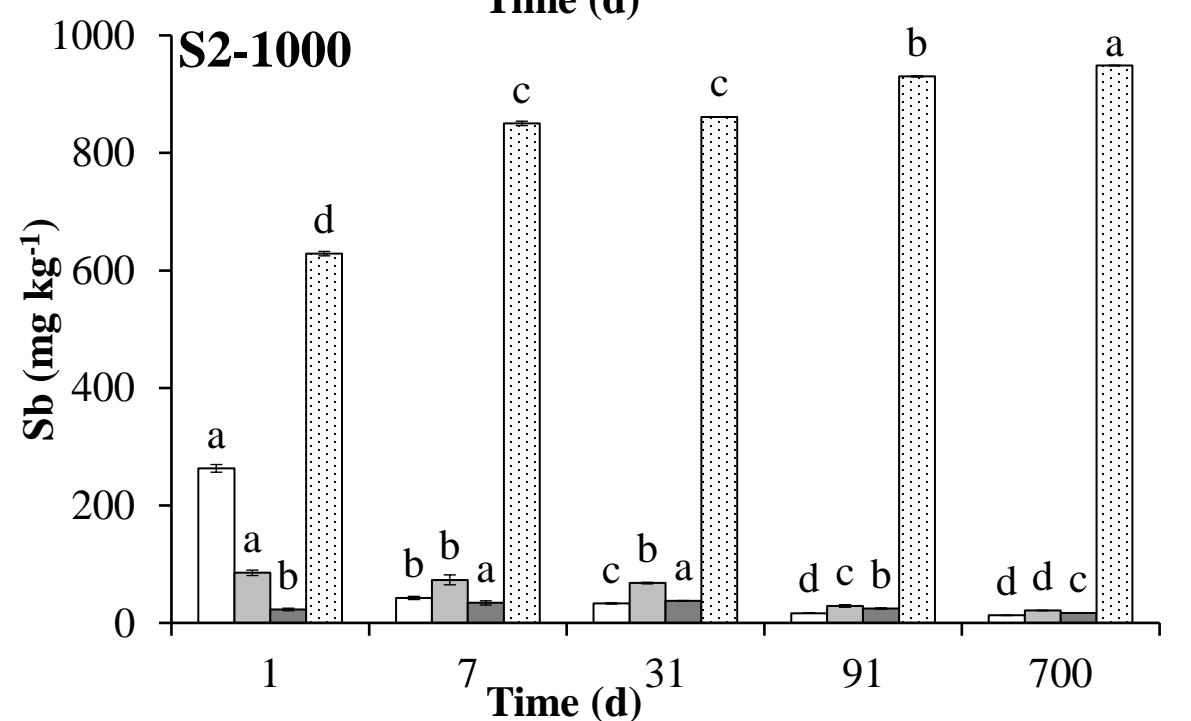
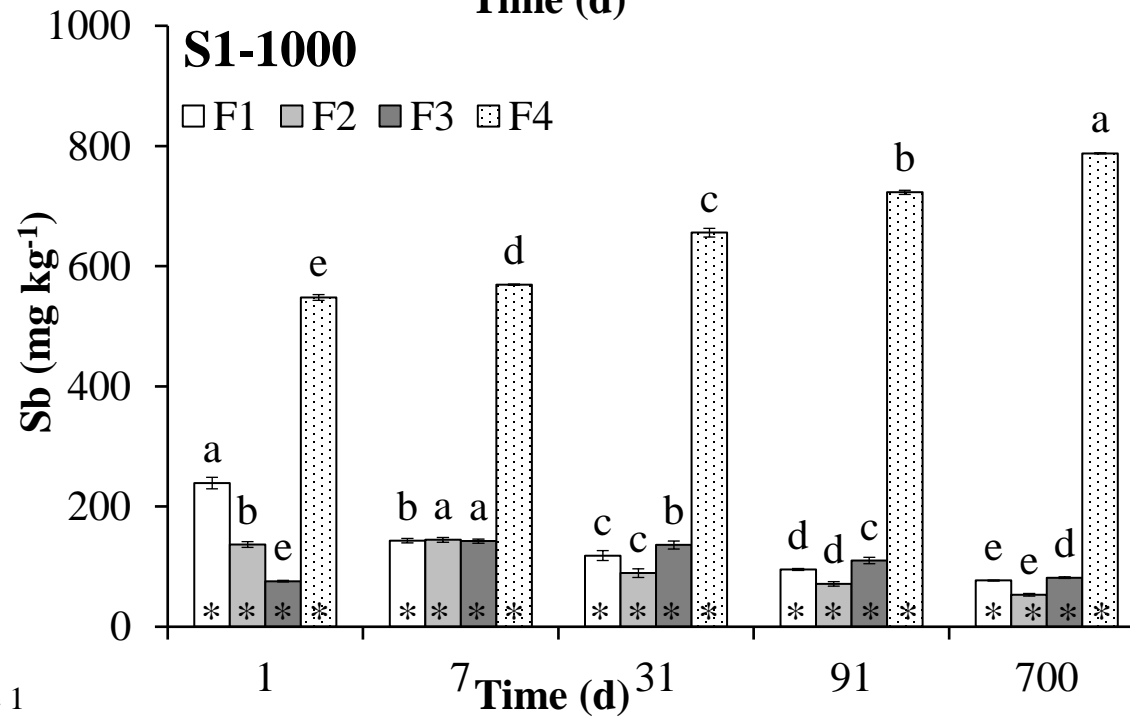
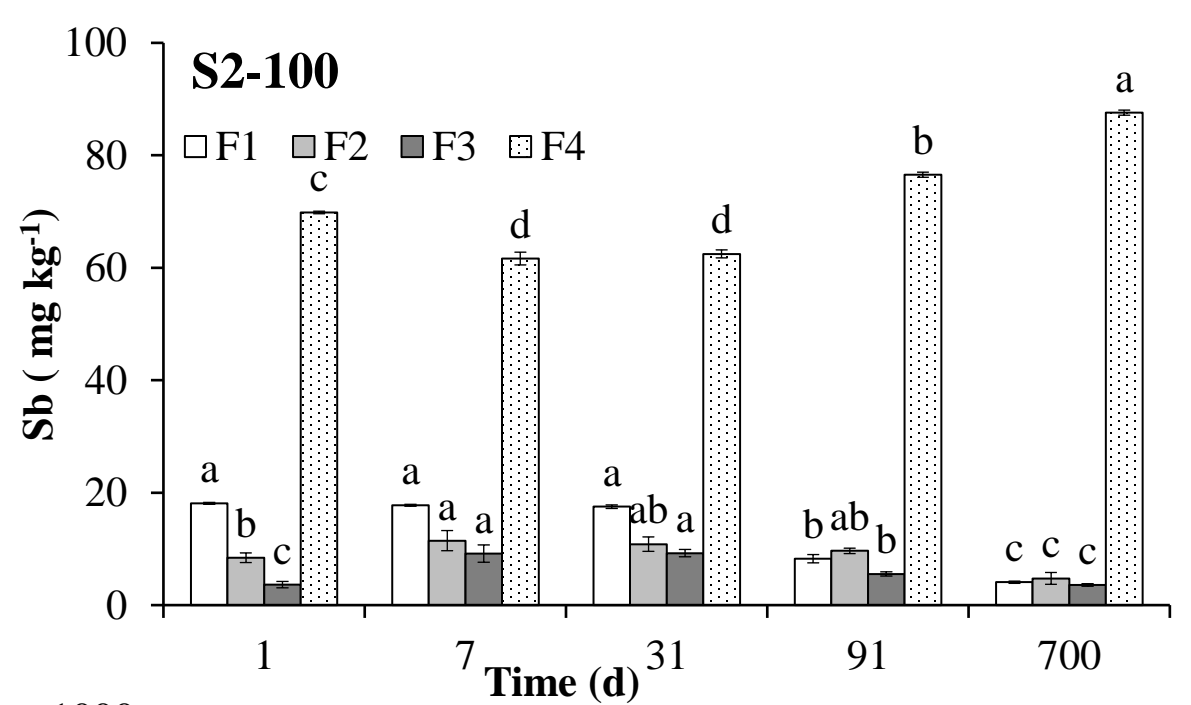
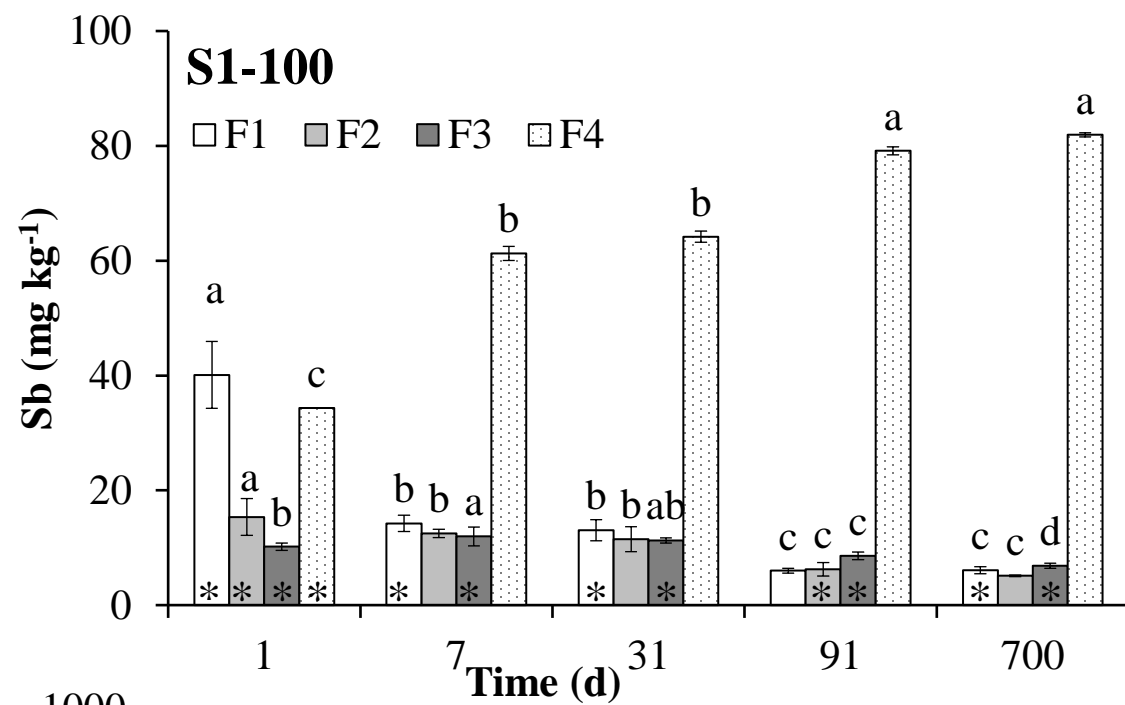


Figure 1

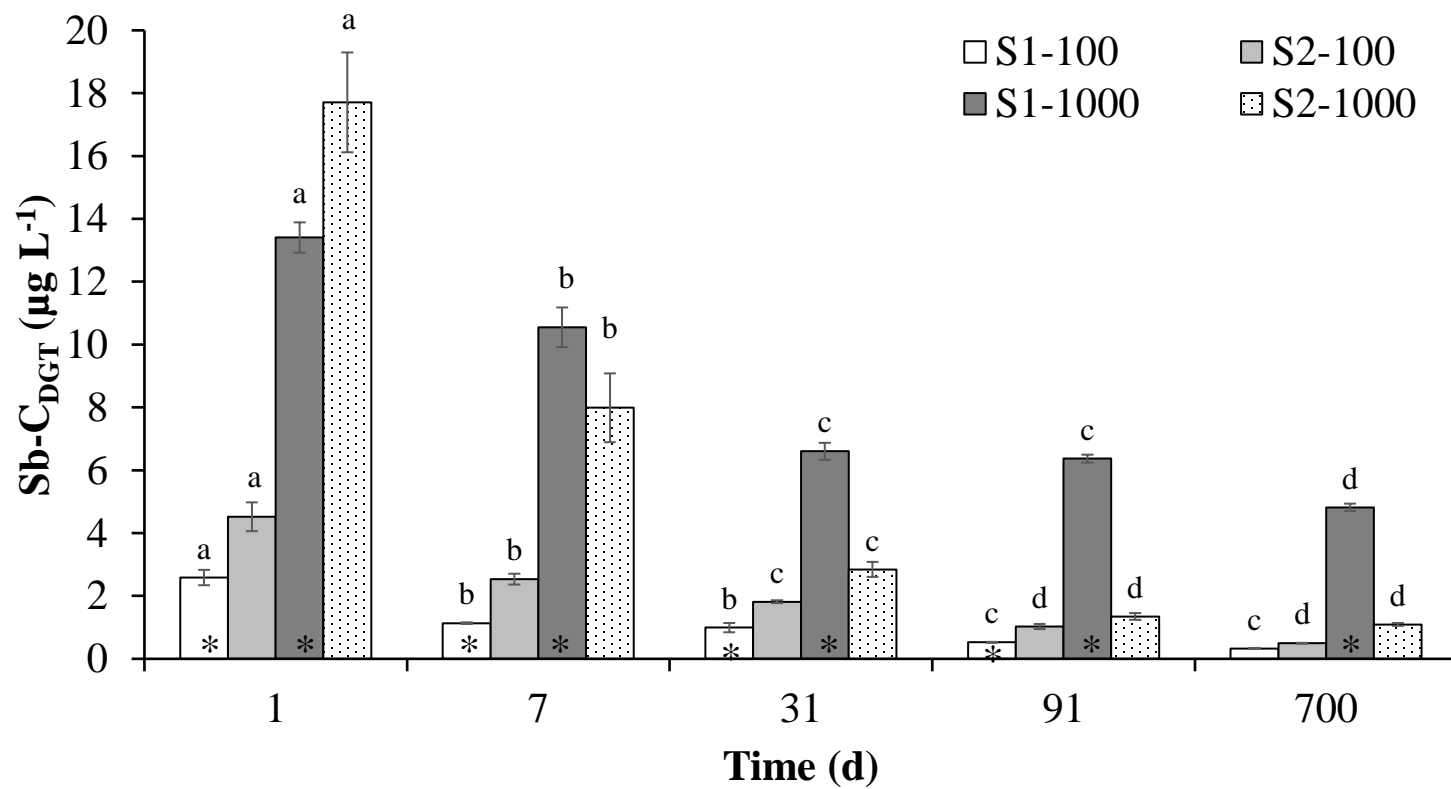


Figure 2



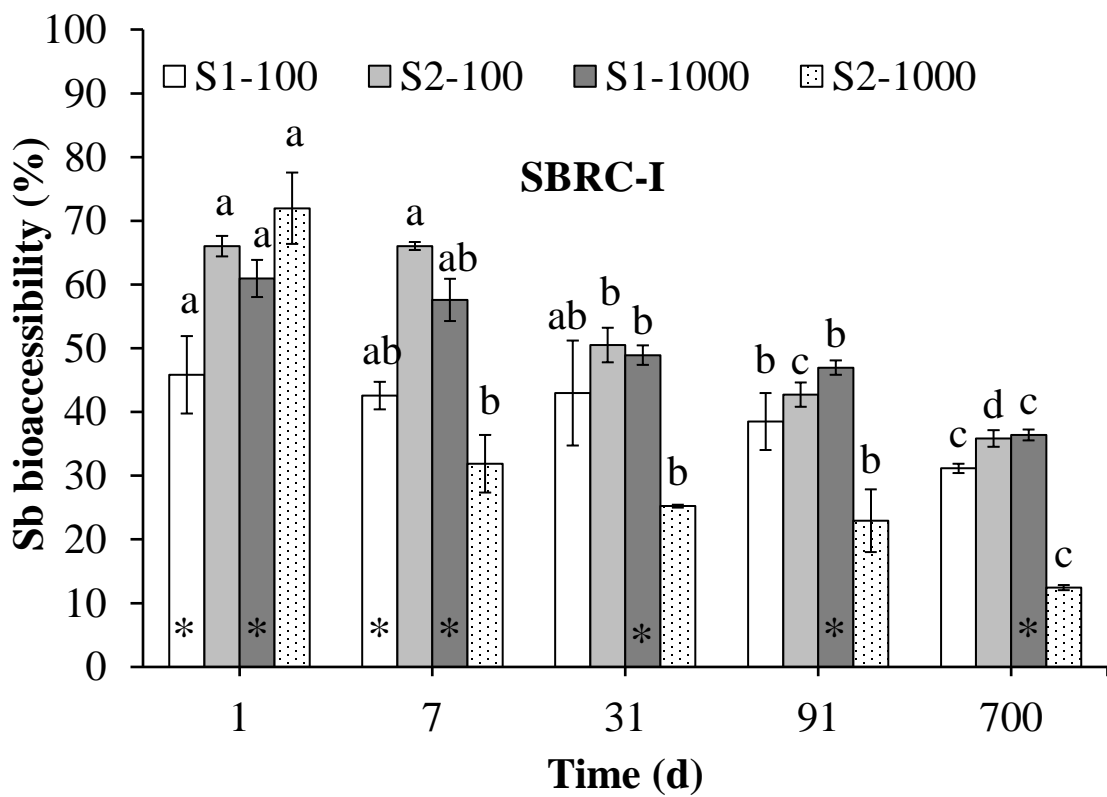
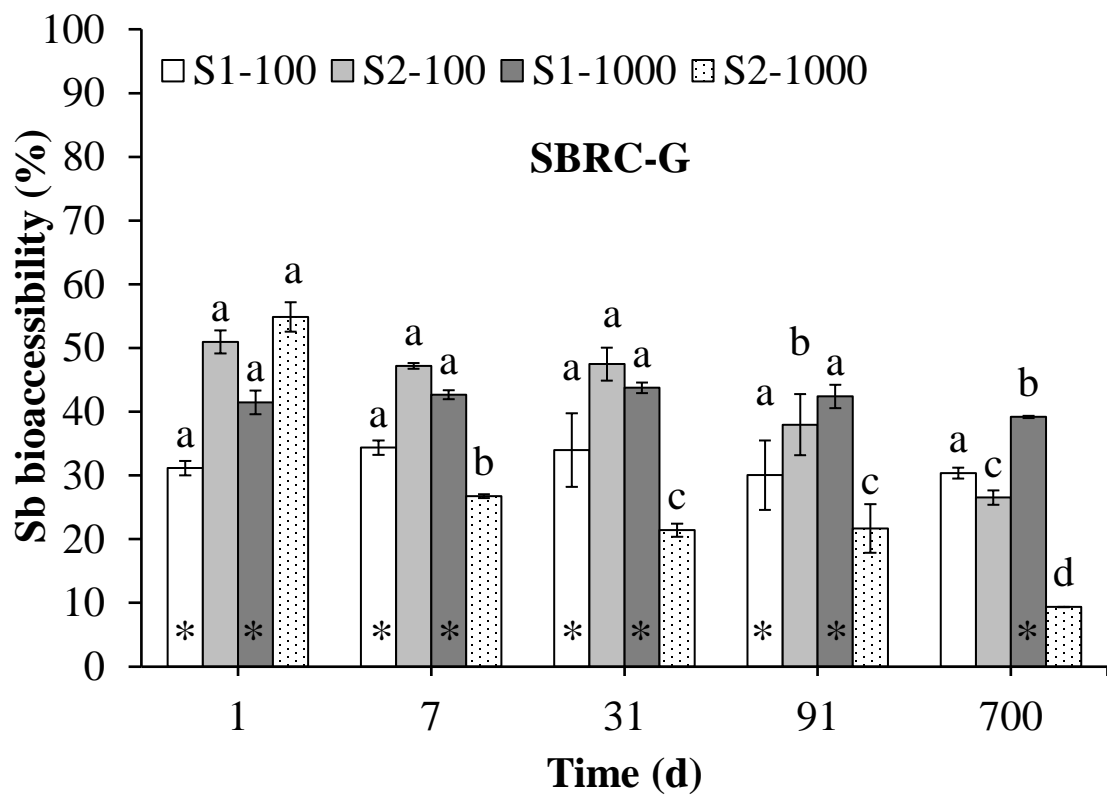
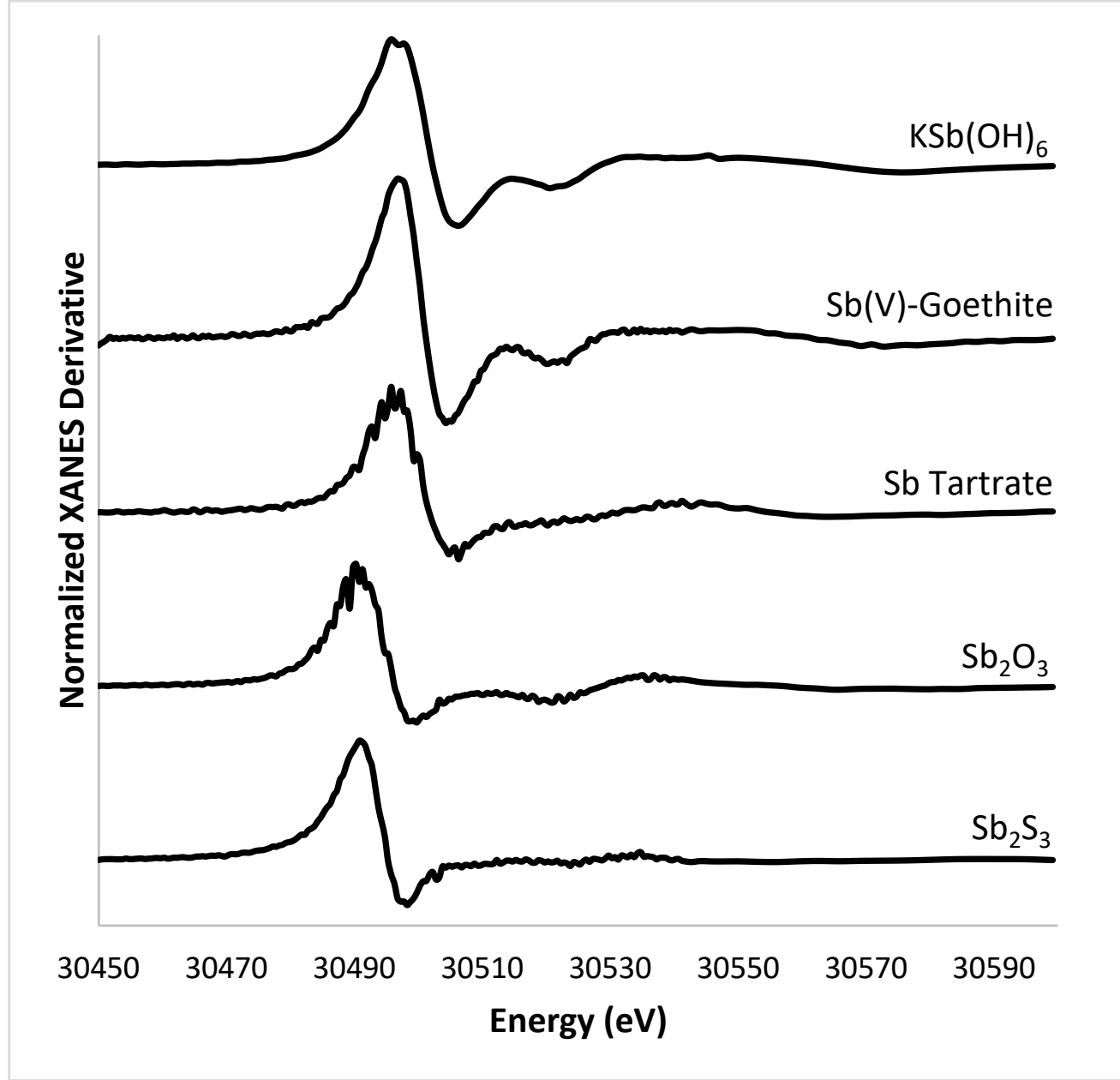


Figure 3

1    **Table S1.** Selected physico-chemical characteristics of S1 and S2 soils.

Physico-chemical parameters	S1 soil	S2 soil
pH <sub>(H<sub>2</sub>O)</sub>	8.2 ± 0.1	4.9 ± 0.2
DOC (mg g <sup>-1</sup> )	0.17 ± 0.00	0.39 ± 0.02
SOM (%)	1.75 ± 0.1	2.19 ± 0.2
CEC (cmol <sub>(+)</sub> kg <sup>-1</sup> )	20 ± 0.8	13 ± 2.5
pH <sub>PZC</sub>	5.7	2.6
Texture <sub>(USDA)</sub>	Sandy clay loam	Loamy coarse sand
<i>Total metal(loid)s (mg kg<sup>-1</sup>)</i>		
Fe	16,350 ± 1,061	5,650 ± 71
Ca	62,500 ± 2,828	2,426 ± 145
Al	19,930 ± 1,018	3,924 ± 749
Sb	n.d.*	n.d.

2    \*n.d., not detected (< 0.01 µg·kg<sup>-1</sup>).



**Figure S1.** Derivative XANES spectra of antimony reference materials considered for linear combination fitting.

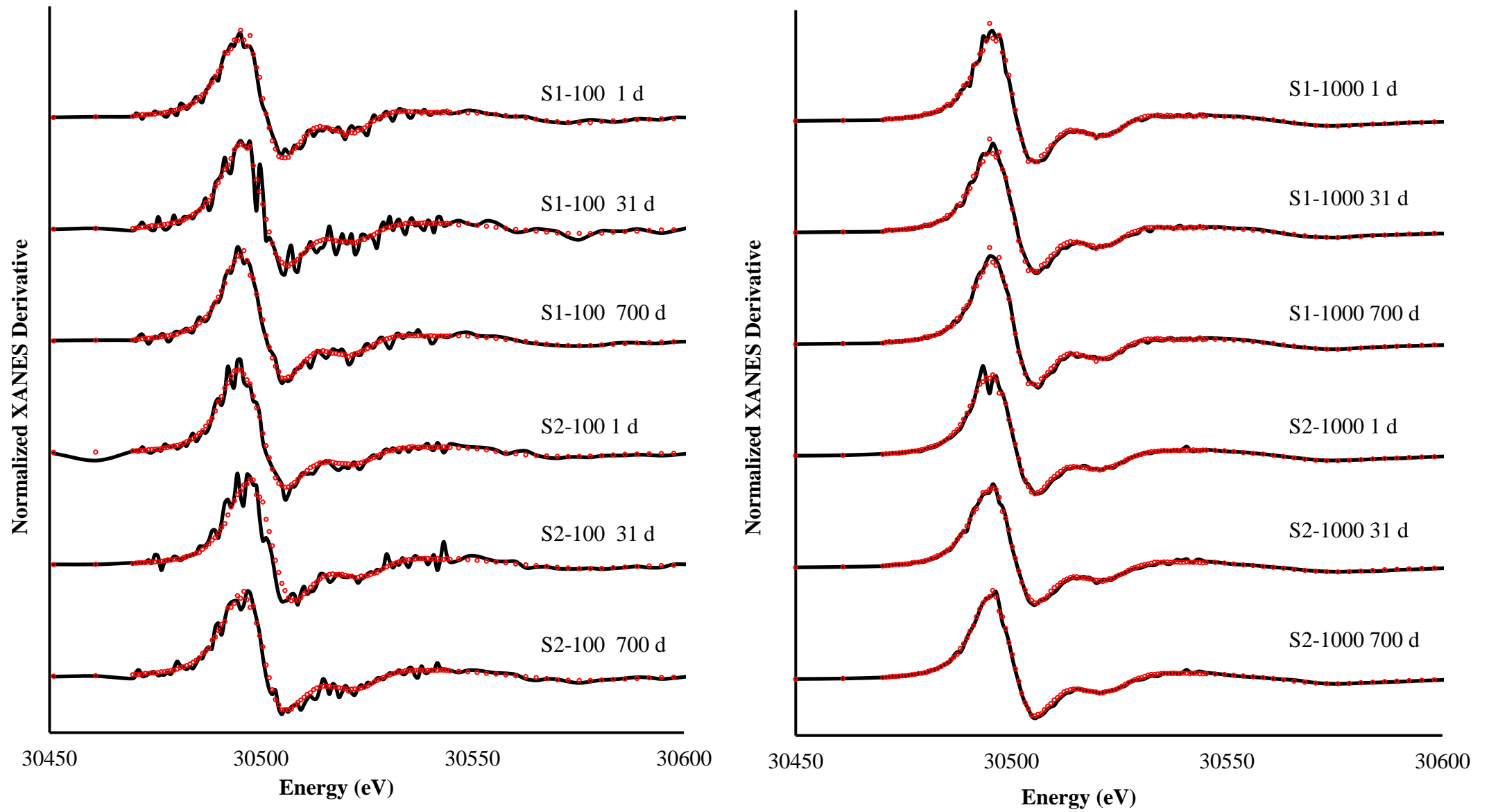


**Figure S2.** Derivative XANES spectra of antimony from S1 and S2 soils spiked with 100 (S-100) and 1000 (S-1000) mg Sb kg<sup>-1</sup> soil at different ageing time. Black curves represent sample data while red curves represent LCF results. Processed results are presented in Table 4.